Computational Energy Science

Vol. 1, No. 2, p. 102-116, 2024

Original article

Study on leakage and diffusion characteristics of Hydrogen-blended natural gas in utility tunnels and ventilation strategies

Chuanyong Zhu[1], Shaoye Zhu[1], Pengfei Duan[2], Luling Li[2], Liang Gong[1]*

[1]*China University of Petroleum (East China), College of New Energy, Qingdao 266580, P. R. China*

[2]*Shenzhen Gas Corporation Ltd, Shenzhen 518049, P. R. China*

Keywords:
Hydrogen-blended natural gas
gas leakage and diffusion
utility tunnels
ventilation strategies

Cited as:
Zhu, C., Zhu, S., Duan, P., Li, L., Gong, L. Study on leakage and diffusion characteristics of Hydrogen-blended natural gas in utility tunnels and ventilation strategies. Computational Energy Science, 2024, 1(2): 102-116.
https://doi.org/10.46690/compes.2024.02.04

Abstract:
Natural gas transportation, storage and distribution systems are relatively well-developed. Hydrogen-blended natural gas (H_2-NG) can utilize the existing infrastructure, reducing the cost of renewal and reconstruction and enabling wide-range hydrogen transportation. However, incorporating hydrogen into natural gas modifies its characteristics, leading to leakage and diffusion behaviors that differ from those of pure natural gas. To examine these characteristics of H_2-NG, this paper numerically simulates the leakage process in a utility tunnel and investigates the influences of leak apertures, hydrogen blending ratios (HBRs), pipeline operating pressure, and ventilation conditions on the gas distribution in the tunnel. The results show that an increase in leak aperture and pipeline pressure leads to higher gas concentration, a larger diffusion radius in the tunnel, and earlier alarm time. The amount of leakage is positively correlated with the HBR; increasing HBR increases the amount of leakage and the risk of explosion in the utility tunnel. Ventilation significantly impacts the gas concentration within the tunnel. With smaller leak apertures and pipeline pressures, 6-12 times per hour mechanical ventilation can reduce the gas concentration in the utility tunnel to a safe range. A ventilation strategy of at least 15 times per hour should be adopted for larger leak sizes and pipeline pressures. The results of this study provide theoretical guidance for managing the leakage process of H_2-NG in underground comprehensive utility tunnels.

1. Introduction

The extensive combustion of fossil fuels has led to critical ecological and environmental challenges, including global warming, acid rain and air pollution. Although natural gas is relatively cleaner, its combustion still produces greenhouse gases, thus impacting climate change. Consequently, the promotion of renewable energy development has become the primary focus of the current energy transition (Apostolou et al., 2019; El-Ghafour et al., 2010; Østergaard et al., 2020, 2020a; Le et al., 2024). Hydrogen has advantages such as being carbon-free, highly efficient and an abundant material supply. Blending hydrogen with natural gas offers a viable pathway to curtail greenhouse gas emissions and minimize environmental repercussions (Ogden et al., 2018; Kong et al., 2021; Tian and Pei, 2023; Kong et al., 2024; Wang et al., 2024). This hybrid approach not only leverages the cleaner combustion of hydrogen but also aligns with ongoing efforts to optimize energy. Under these circumstances, the transport of hydrogen-blended gas (H_2-NG) is gaining escalating significance. In recent years, the integration of gas pipelines into underground utility tunnels has rapidly developed. Laying gas pipelines in these enclosed underground spaces and setting up fire barriers effectively prevent damage to the gas pipelines (Wu et al., 2021; Wang et al., 2021; Zhao et al., 2022). However, due to the significant differences in physical properties between hydrogen and natural gas, the leakage and diffusion characteristics of H_2-NG can markedly differ from those of natural gas alone. This may lead to differences in emergency response measures and fire risk assessments following the leaking of the two types of gas (Sun and Guo, 2024). Consequently, understanding the dynamic

Yandy Scientific Press

*Corresponding author.
E-mail address: cyzhu@upc.edu.cn (C. Zhu); zsy990329@163.com (S. Zhu); duanpf@szgas.com.cn (P. Duan); lill05@szgas.com.cn (L. Li); lgong@upc.edu.cn (L. Gong).

Received April 10, 2024; revised May 16, 2024; accepted June 16, 2024; available online June 19, 2024.

characteristics of leakage and diffusion for the H_2-NG in these tunnels, as well as implementing necessary response measures such as enhanced ventilation, is crucial for mitigating risks.

Extensive research has been conducted on the dynamics of flammable gas leaks across various environments, highlighting the behavior of flammable gases under different conditions. Studies by Choi et al. (2013) and Kim et al. (2013) provide significant insights into hydrogen leak scenarios in underground parking garages of fuel cell vehicles and refueling stations, respectively, offering predictive models for hydrogen concentration evolution. Similarly, some research also delves into leakage dynamics, the influence of factors, such as leak aperture and wind speeds, on gas diffusion and the formation of hazardous zones. For instance, Yu et al. (2022) analyzed the leakage and diffusion of natural gas pipelines, examining the effects of leakage rate, leak aperture and wind speed on the hazardous boundary of gas diffusion. Mei et al. (2022) explored natural gas leakage in typical building layouts, discovering that high wind speeds ($\geq$ 6 m/s) create reverse vortices due to wind shear, causing natural gas clouds to descend. Qian et al. (2020) utilized hydrogen refueling stations in China as a case study to investigate hydrogen leakage and diffusion under varying conditions, providing a quantitative analysis of the combustible gas cloud distribution resulting from leaks. Additional studies have also explored specific aspects of gas leak dynamics and safety hazards, such as instantaneous leakage responses, explosion hazards and alarm response times in residential and industrial settings. Specifily, Abdas et al. (2020) studied the instantaneous leakage of hydrogen in enclosed gas cylinder chambers, including the formation of hazardous zone heights and the time for the complete disappearance of hazardous zones under different conditions of leak apertures and positions, and they marked high-risk states. Su et al. (2022) investigated explosion hazards, alarm response times and gas concentration distributions in household kitchens, assessing the impact of hydrogen blend ratio, leakage rate and leak aperture on the characteristics of gas leakage.

Despite extensive research, there remains a significant gap in comprehensive research specifically addressing the leakage and diffusion characteristics of H_2-NG blends in utility tunnels. Although studies like those of Liu et al. (2023), Zhou et al. (2022) and Wang et al. (2020) have explored the diffusion characteristics, sensor networks and simulation models for natural gas leaks in utility environments. Yet, the unique properties of H_2-NG blends, such as increased diffusivity and altered flammability limits, necessitate more targeted research. Limited work, such as the study by Shao et al. (2022), has begun to address this issue. They conducted an in-depth investigation in a Shanghai utility tunnel, comparing the leakage and diffusion behaviors of hydrogen and natural gas. Their findings indicate that greater diffusivity of hydrogen renders current ventilation standards designed for natural gas, inadequate. This underscores the urgent need to develop specific safety protocols for H_2-NG blends in confined spaces. However, this part of the work still appears insufficient, pointing to a critical need for expanded research to comprehensively address these complex challenges.

Overall, while there have been numerous studies on the leakage and diffusion characteristics of natural gas and hydrogen in specific scenarios, comprehensive research specifically addressing the leakage and diffusion characteristics of H_2-NG in underground utility tunnels is relatively scarce. Furthermore, there is a notable lack of effective ventilation strategies to ensure safe gas concentration levels in H_2-NG utility tunnels after the gas leakage. Therefore, this paper seeks to bridge these gaps by conducting a detailed numerical study of the leakage and diffusion behavior of H_2-NG in underground utility and assessing the impact of factors like leak aperture, pipeline pressure, HBR and ventilation strategies on hazardous area distribution patterns, the time of alarm and the time achieving to the lower explosion limit (LEL) after the leakage. This research aims to provide a theoretical basis for the secure operation of H_2-NG. The paper is structured as follows: the second section outlines the physical model and the theory of the numerical simulation; the third section analyzes the effects of various factors on the leakage and diffusion behavior of H_2-NG; and the final section summarizes the findings of the study.

2. Physical model and governing equations

2.1 Physical model

In this study, the utility tunnel being examined has a total length of 200 m with a cross-sectional of 1.5 m $\times$ 3.0 m, as depicted in Fig. 1. The tunnel's base is supported by pillars and a gas pipeline with a diameter of 0.3 m is installed above these pillars. The leak point is situated at the midpoint of the pipeline, 100 m from the entrance of the tunnel. To replicate the ventilation conditions in the tunnel after the leak, air outlets and inlets are positioned at the ceiling of the tunnel, each with a dimension of 1 m $\times$ 1 m. In order to investigate the diffusion radius of gas in the tunnel after a leak, two lines are defined along the length of the tunnel. One is located at the central height of the tunnel, located 1.5 m from the bottom and the other is a monitoring line located 0.6 m from the top. According to the literature (Wang et al., 2022), gas monitoring points are installed at the top of the tunnel, spaced 15 m apart and positioned 0.5 m below the ceiling of the tunnel. The gas alarm threshold is 20% of the lower explosive limit, as listed in Table 1.

Table 1. The lower explosion limit (LEL) and alarm concentration at different HBRs

HBR (%)	Alarm concentration (%)	LEL (%)
0	1.00	5.00
10	0.98	4.88
20	0.95	4.76
30	0.94	4.70

2.2 Governing equations

In developing the mathematical model for gas leakage and diffusion in the utility tunnel described earlier, this pa-

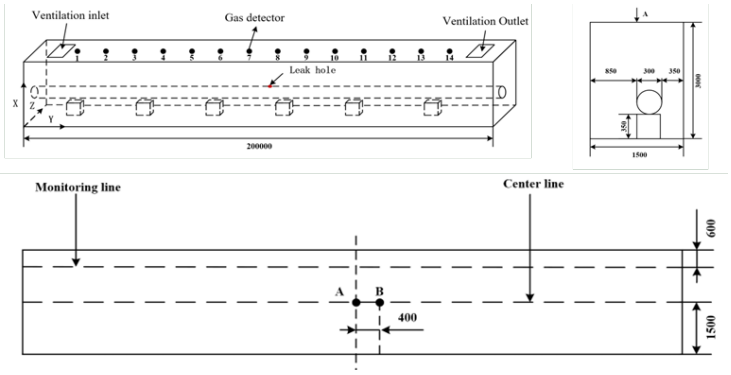

Fig. 1. Physical model of the utility tunnel, the layout of monitoring points and the schematic diagram of A cross-section (mm).

per employs certain simplifications and assumptions. These include treating both the gas and air as ideal gases and assuming no chemical reactions between the leaking gas and air. The gas flow is considered to be turbulent. It is also assumed that the mass leakage rate of the gas is constant throughout the leakage process and the wind speed is stable under ventilation conditions. Given these simplifications and assumptions, the control equations to this problem comprise the continuity equation, the momentum equation, the species transport equation and the turbulence model.

Continuity equation (Li et al., 2022):

$$\frac{\partial \rho}{\partial t}+\frac{\partial \rho u_i}{\partial x_i}=0 \tag{1}$$

Momentum equation (Yu et al., 2022):

$$\frac{\partial(\rho u)}{\partial t}+\frac{\partial(\rho u^2)}{\partial x}=-g\rho\sin\theta-\frac{\partial p}{\partial x}-\frac{\lambda}{D}\frac{u^2}{2}\rho \tag{2}$$

Energy equation (Yu et al., 2022):

$$-\rho u\frac{\partial H}{\partial x}=\frac{\partial}{\partial t}\left[\rho\left(e+\frac{u^2}{2}+gz\right)\right]+\frac{\partial}{\partial x}\left[\rho u\left(h+\frac{u^2}{2}+gz\right)\right] \tag{3}$$

Species transport equation (Su et al., 2022):

$$\frac{\partial(\rho c_s)}{\partial t}+\frac{\partial}{\partial x_i}(\rho u_i c_s)=\frac{\partial}{\partial x_i}\left(D_{air-s}\rho\frac{\partial c_s}{\partial x_i}\right) \tag{4}$$

where ρ is the fluid density, kg/m^3; g is the gravity acceleration, m/s^2; t is time, s; u_i is the velocity in the i direction, m/s; λ is the friction factor along the pipeline; θ is the angle between the pipeline and the horizontal plane, °; L is the internal diameter of the pipeline, m; p is the gas pressure inside the pipeline, pa; H is the heat released per unit mass of gas, J/kg; h is the enthalpy of the gas, J/kg; e is the internal energy of the gas, J/kg; z is the height of the pipeline position, m; s represents the gas species; C_s is the volume concentration of species s; D_{air-s} is the diffusion coefficient of species s in air, m^2/s. As in Li et al. (2021), $D_{air-\mathrm{H_2}}$ = 7.6×10^{-5} m^2/s and $D_{air-\mathrm{CH_4}}$ = 1.6×10^{-5} m^2/s.

This paper employs the Realizable $k-\varepsilon$ turbulence model (Liu et al., 2009). This model incorporates the equations for turbulent kinetic energy and turbulent dissipation rate.

$$\begin{aligned}&\frac{\partial}{\partial t}(\rho k)+\frac{\partial}{\partial x_j}(\rho k u_j)\\&=\frac{\partial}{\partial x_j}\left[\left(\mu+\frac{\mu_l}{\sigma_k}\right)\cdot\frac{\partial k}{\partial x_j}\right]+G_k+G_b+\rho\varepsilon-Y_M+S_k\end{aligned} \tag{5}$$

$$\begin{aligned}&\frac{\partial}{\partial t}(\rho\varepsilon)+\frac{\partial}{\partial x_j}(\rho\varepsilon u_j)\\&=\frac{\partial}{\partial x_j}\left[\left(\mu+\frac{\mu_l}{\sigma_\varepsilon}\right)\cdot\frac{\partial \varepsilon}{\partial x_j}\right]+\rho C_1 S_\varepsilon-\rho C_2\frac{\varepsilon^2}{k+\sqrt{v\varepsilon}}\\&\quad+C_1\frac{\varepsilon}{k}C_3 G_b+S_\varepsilon\end{aligned} \tag{6}$$

where μ and μ_t are the dynamic viscosity coefficient and the eddy viscosity coefficient, Pa·s, respectively; G_k represents the turbulent kinetic energy generated by velocity gradients, kg·m^{-1}·s^{-3}; G_b is the production term of turbulent kinetic energy caused by buoyancy, kg·m^{-1}·s^{-3}; β is the thermal expansion coefficient; YM is the fluctuation caused by excessive dissipation in compressible turbulence, kg·m^{-1}·s^{-3}; M_t is the Mach number; σ_k and σ_ε are the turbulent Prandtl numbers for the k and ε equations, respectively; S_k is a user-defined source term. C_1 and C_2 are constants and $C_1=\max[0.43,\eta/(\eta+5)]$, $\eta=S\cdot(k/\varepsilon)$, $S=\sqrt{2S_{ij}S_{ij}}$.

The boundary conditions are defined as follows: the leak aperture is modeled as a pressure inlet. The outlet is connected to the atmosphere and set as a pressure outlet at ambient pressure; the walls of the utility tunnel and the pipeline are set as no-slip surfaces. Besides, to simulate the diffusion process of H_2-NG in the utility tunnel, a species transport model is used without considering chemical reactions, and the turbulence is modeled using the Realizable $k-\varepsilon$ model. Standard wall functions are applied to the walls, and the species are modeled using a first-order upwind scheme, while energy, density and turbulence are modeled using a second-order upwind scheme. The time step is set as 0.01 s, the iterative step is 100 and the calculation time is 100 s.

2.3 Grid independence validation

The gas leakage model encompasses various regions, such as the core jet area and the diffusion area. Given the disparity between the overall dimensions of the utility tunnel and the leak aperture, local refinement of mesh is imperative. A high-

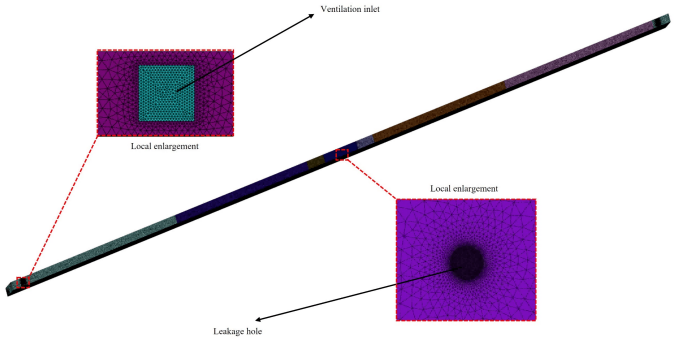

Fig. 2. Grid details of the utility tunnel.

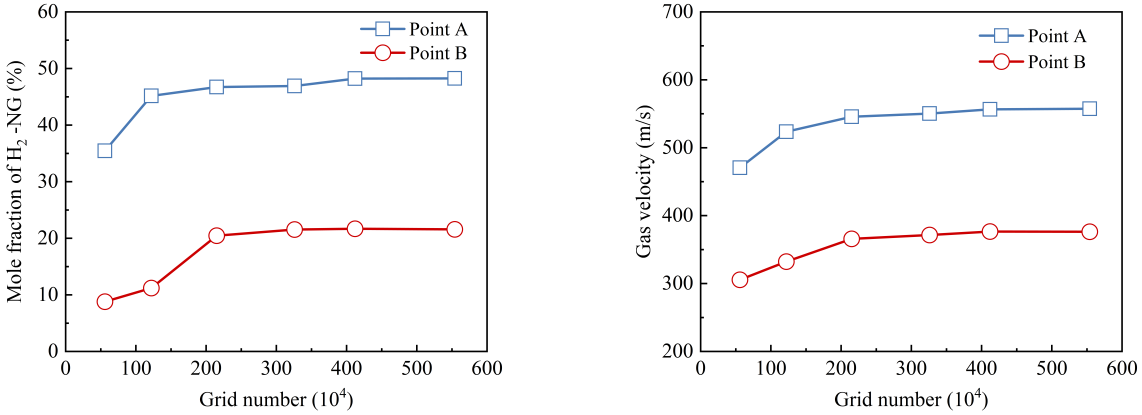

(a) Mole fraction of H_2-NG (b) Gas velocity

Fig. 3. Grid independence validation.

density grid is employed in the core jet area to capture detailed flow dynamics, while a low-density grid is utilized in regions further from the core jet area to optimize the balance between computational accuracy and resource allocation. The detailed grid information is shown in Fig. 2.

Grid independence in the model is verified by analyzing the mole fraction of the leakage gas and the gas velocity in different positions. The model was tested with different numbers of grid cells, including 0.56, 1.22, 2.15, 3.26, 4.12 and 5.54 million. As illustrated in Fig. 3, the improvement in computational accuracy for both the mole fractions of the gas and gas velocities becomes negligible beyond 4.12 million cells. Consequently, to achieve the desired accuracy while enhancing computational efficiency, the model employing 4.12 million cells is selected for the computational analyses in subsequent parts of the study.

2.4 Parameters setting and model validation

Before beginning this research, it is essential to clarify the settings of various parameters. The operating pressure of a pipeline significantly affects the gas diffusion pattern following a leak, and for the purposes of this study, we have classified these pressures into medium, sub-high and high categories. We have chosen specific pressures of 0.4, 0.8, 1.0 and 1.6 MPa to simulate the leakage and diffusion processes at these varied pressure levels. Another important variable, the size of the leak aperture, influences the leak dynamics. Based on the literature EIA (2020), apertures smaller than 6.35 mm are classified as small holes. Consequently, we selected a 2 mm diameter for small hole leak conditions, and 8 mm and 12 mm diameters for scenarios involving larger leaks. Additionally, while most studies on the H_2-NG gas diffusion process consider a maximum hydrogen blending ratio of 20% (Su et al., 2022), we examined ratios of 0%, 10% and 20%, and extended our analysis to 30% to explore the effects of higher hydrogen concentrations on the diffusion of leaked gas. The ventilation conditions within pipeline galleries are also a critical safety factor. According to the guidelines stated in Liu (2018), ventilation requirements for pipeline leakage incidents must exceed 12 times/h. In this study, 3 times/h and 6 times/h ventilation rates were selected for conditions that do not meet these emergency ventilation standards, while ventilation rates of 12, 15 and 18 times/h were selected to investigate gas distribution under high-frequency ventilation conditions. This approach allows us to thoroughly assess the impact of different ventilation frequencies on gas distribution, ensuring safety and efficiency in emergency scenarios. All conditions were conducted at 300 K. The simulated conditions,

Table 2. Simulated conditions and parameters.

Case	pipeline pressure (MPa)	leakage rate (kg/s)	leak apertures (mm)	ventilation rate (times/h)	HBR (%)
1	0.4	1.95×10^{-3}	2	0	20
2	0.8	0.06226	8	0	20
3	0.8	0.14009	12	0	20
4	0.8	3.89×10^{-3}	2	0	0
5	0.8	3.89×10^{-3}	2	0	10
6	0.8	0.06226	8	0	20
7	0.8	3.89×10^{-3}	2	0	20
8	0.8	3.89×10^{-3}	2	0	30
9	0.8	3.89×10^{-3}	2	3	20
10	0.8	3.89×10^{-3}	2	6	20
11	0.8	3.89×10^{-3}	2	12	20
12	1.0	3.89×10^{-3}	2	0	20
13	2.0	0.00973	2	0	20
14	2.0	0.35025	12	12	20
15	2.0	0.35025	12	15	20
16	2.0	0.35025	12	18	20

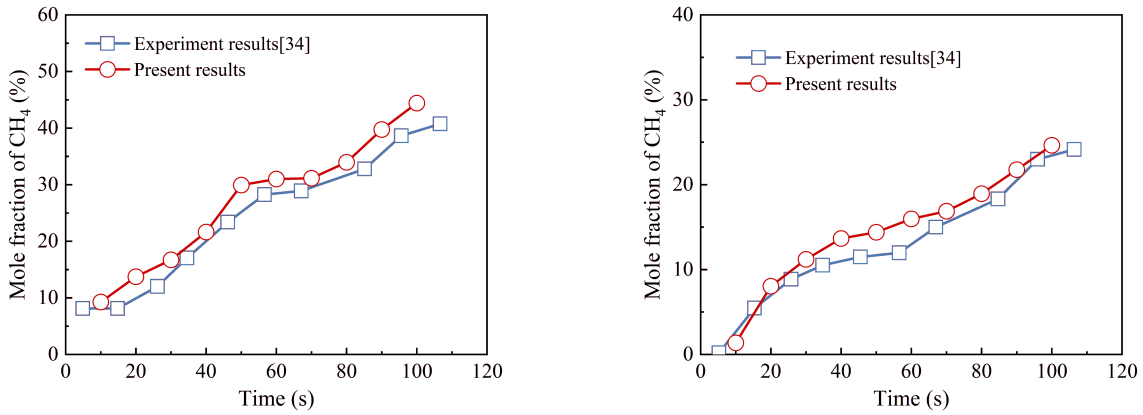

(a) Monitoring point 2 (b) Monitoring point 4

Fig. 4. Comparisons between the present results and available experimental results in Liu (2018).

considering all these factors, are provided in Table 2. In this Table the leakage rate of gas can be given as (Liu, 2018):

$$q_0 = C_0 A_0 P_2 \sqrt{\frac{kM}{ZRT} \cdot \left(\frac{2}{k+1}\right)^{\left(\frac{k+1}{k-1}\right)}} \tag{7}$$

where C_0 represents the leakage coefficient, with a value of 1 for circular holes and 0.9 for rectangular holes; A_0 represents the area of the leakage hole in square meters, m^2; k represents the adiabatic index of the gas; M represents the Mach number; R represents the gas constant in $J\cdot kg^{-1}\cdot K^{-1}$; T represents the gas temperature, K; Z represents the compression factor.

To validate the accuracy of the model in this paper, the calculated results of natural gas mole fraction in the utility tunnel were compared with the available experimental data Ref. Liu (2018), as displayed in Fig. 4. In the numerical simulations, all the conditions are set as described in Ref. Liu (2018), and the natural gas mole fractions at monitoring points 2 and 4 shown in Fig. 1 were obtained. Fig. 4 shows that the simulated results are consistent with the variation trends of the available experimental results, with an average error of less than 10%, indicating that the model established in this paper is reliable.

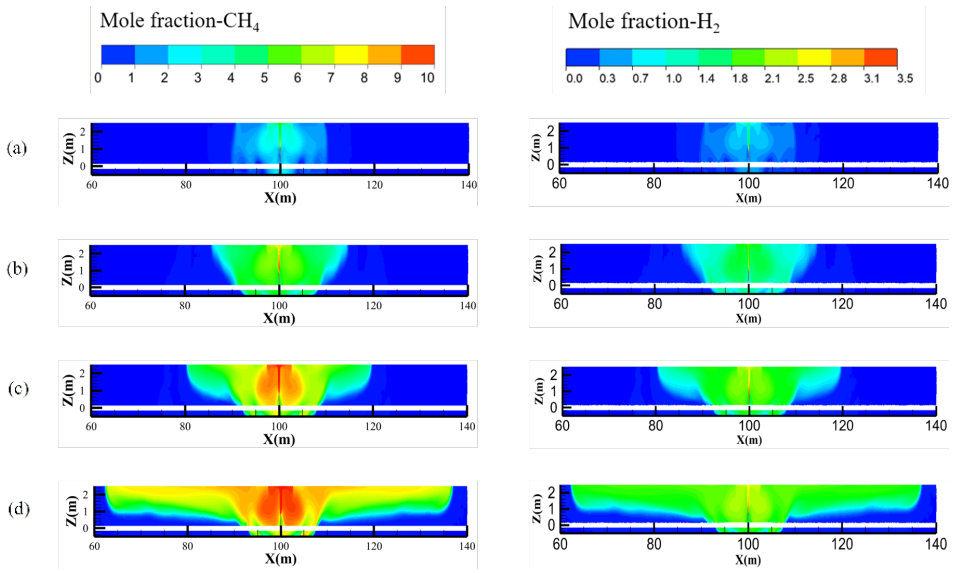

Fig. 5. The distribution of natural gas and hydrogen at different leakage times without mechanical ventilation: (a) t = 10 s; (b) t = 30 s; (c) t = 50 s; (d) t = 100 s.

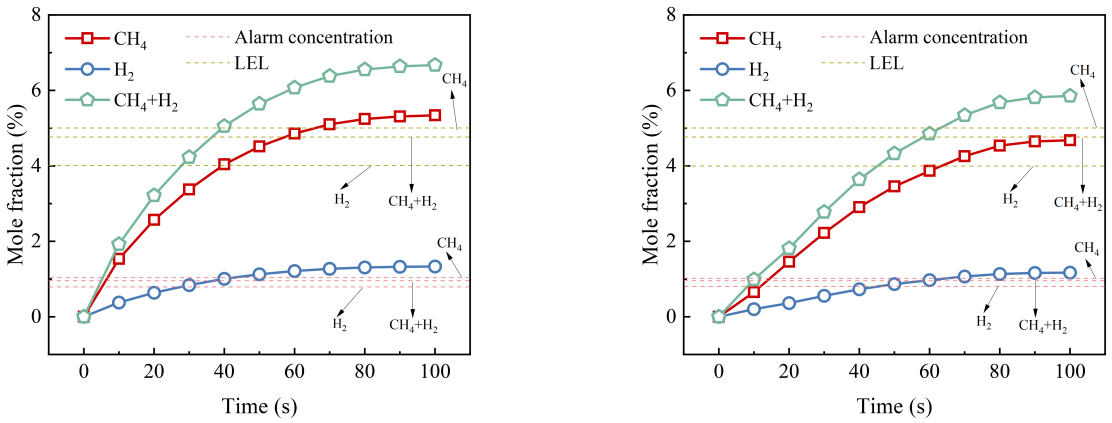

(a) Monitoring point 8 (b) Monitoring point 9

Fig. 6. The distribution of leaking gas at different monitoring points without mechanical ventilation (Alarm concentration and LEL line from top to bottom as CH_4, CH_4+H_2, H_2).

3. Results and discussion

3.1 Diffusion process of H_2-NG in the utility tunnel

Fig. 5 presents the distribution of natural gas and hydrogen in the utility tunnel at different times, given a scenario with a 20% HBR, a 12 mm leak aperture, pipeline pressure at 0.8 MPa, and the absence of ventilation (case 3 in Table 2). The figure reveals that the H_2-NG is ejected at high velocity from the leak hole, leading to rapid accumulation of the H_2-NG at the top of the tunnel, from where it symmetrically diffuses towards both ends. The mole fractions of both natural gas and hydrogen are observed to be higher in the upper region of the tunnel compared to the lower region. This phenomenon is attributable to the fact the inertia of the gas jetting from the small hole causes it to rise and accumulate at the ceiling of the tunnel. Upon impact with the ceiling of the tunnel, the gas rapidly spreads outward, effectively enlarging the diffusion radius. Under the no-mechanical ventilation condition, the gas is symmetrically distributed around the leak hole within the tunnel. Over time, the concentration of the gases at any given location within the tunnel progressively increases, and the radius of diffusion increases, leading to an expansion of the hazardous area along the length of the tunnel.

Fig. 6 illustrates the gas concentration distribution at monitoring points 8 and 9 in the utility tunnel under no mechanical ventilation conditions. From Fig. 6(a), it is evident that at monitoring point 8, located near the leak hole, both the H_2-NG and natural gas concentrations rapidly escalate to the alarm level within a mere 4-6 s. This quick accumulation is

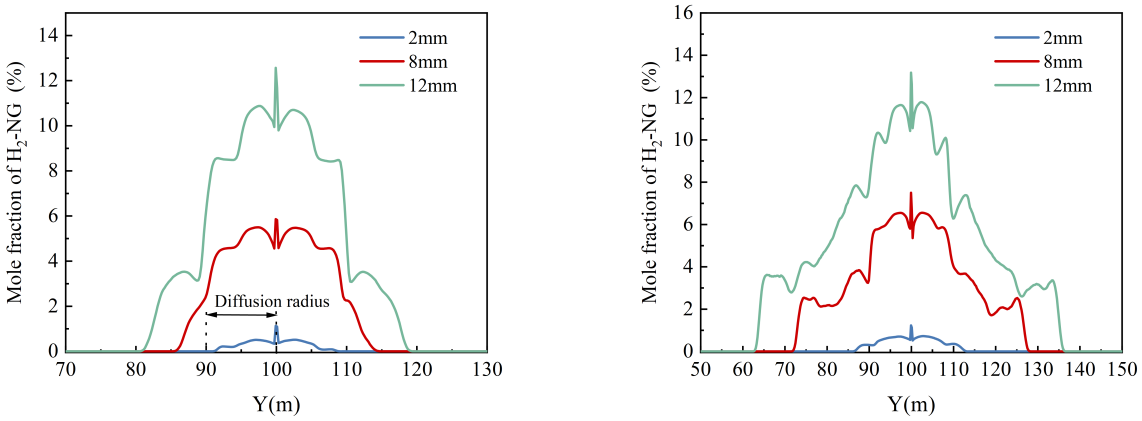

(a) t = 50 s (b) t = 100 s

Fig. 7. The H_2-NG distribution in the centerline under different leak apertures.

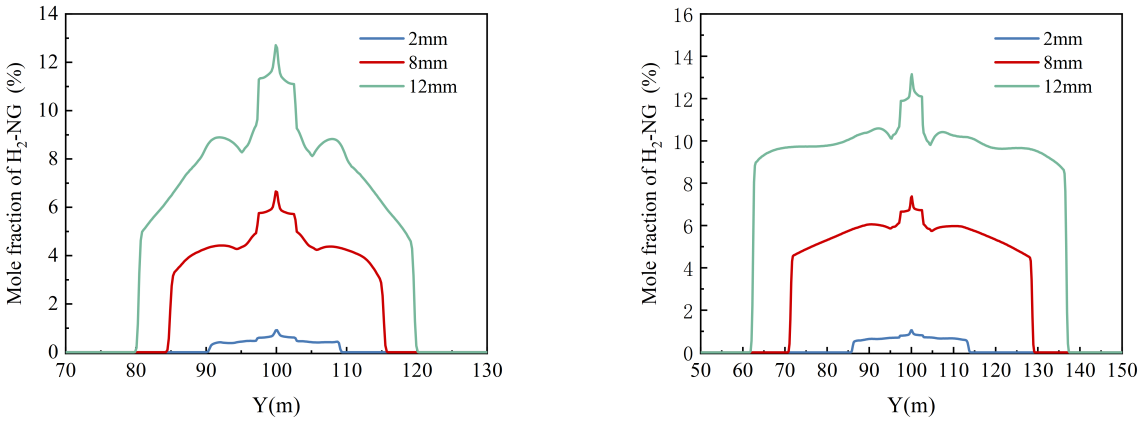

(a) t = 50 s (b) t = 100 s

Fig. 8. The H_2-NG distribution of monitoring line under different leak apertures.

attributed to the high jet velocity of the leaking gas. As the leak progresses, at about 39 s and 68 s, the mole fractions of both the H_2-NG and natural gas surpass the LEL, ultimately stabilizing at 6.6% and 5.3%, respectively. Conversely, as shown in Fig. 6(b), monitoring point 9, which is further from the leak hole, records a lower mole fraction of the leaking gas compared to point 8. At this point, the H_2-NG reaches the LEL at 60 s, while natural gas nears the LEL at about 100 s. These observations indicate that under no mechanical ventilation conditions, the mole fractions of H_2-NG at both monitoring points 8 and 9 attain the LEL within the first 60 s, thereby presenting a significant explosion hazard.

3.2 The influence of leak apertures

This section delves into the leakage and diffusion properties of H_2-NG under no mechanical ventilation conditions and different leak apertures. The specific conditions under consideration involve a pipeline pressure of 0.8 MPa and an HBR of 20%. This study examines three different leak diameters: 2, 8 and 12 mm, which correspond to cases 2, 3 and 7, respectively, as outlined in Table 2.

Figs. 7 and 8 illustrate the variation in the H_2-NG mole fraction along the central and monitoring lines under different leak apertures. As depicted in Fig. 8, the mole fraction of the H_2-NG gradually increases over time, along with an expanding diffusion radius. Figs. 7(a) and 8(a) indicate that the distribution patterns of the leakage gas along both the central and monitoring lines are essentially consistent at the same time intervals. With increasing leak aperture, there is a corresponding increase in the mole fraction of H_2-NG and its diffusion radius. This is attributed to the fact that larger leak apertures result in greater quantities of H_2-NG being released, leading to a higher mole fraction in the utility tunnel. Furthermore, directly above the leak hole, the mole fraction of H_2-NG reaches its maximum, forming a peak. This peak is due to the area above the leak hole, where the leakage speed

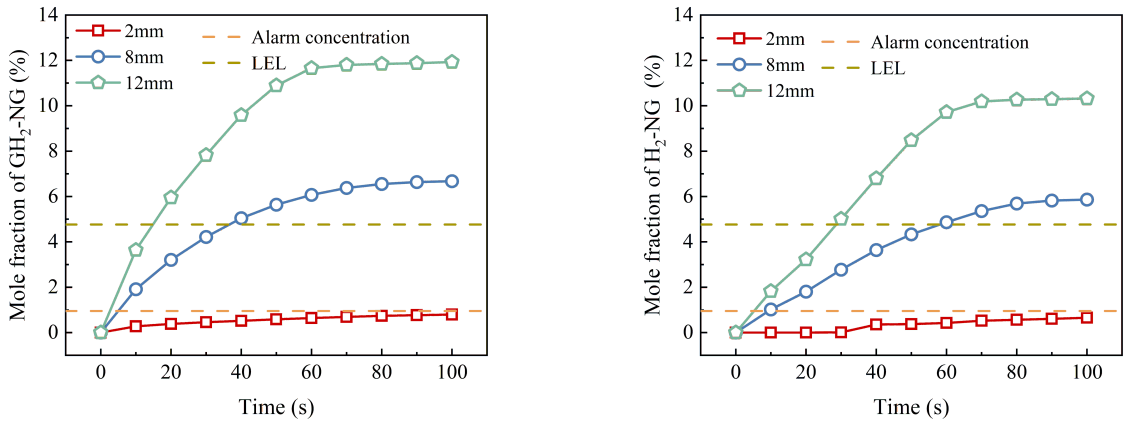

(a) Monitoring point 8 (b) Monitoring point 9

Fig. 9. Effect of leakage aperture on the concentration of H_2-NG.

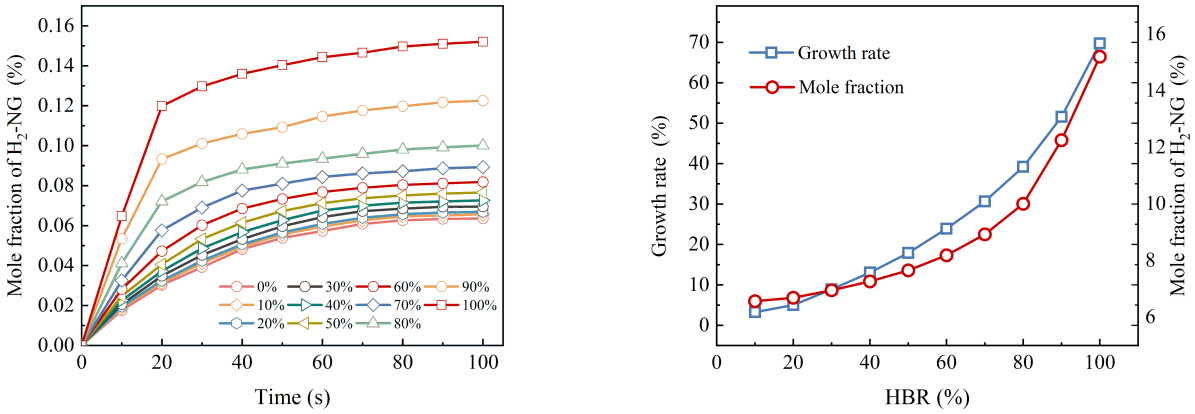

(a) The concentration of H_2-NG varies with time under HBRs at monitoring point 8

(b) The concentration and growth rate of H_2-NG varies with HBR at t = 100 s of monitoring point 8

Fig. 10. The effect of HBRs on H_2-NG concentration and leak speed growth rate.

of H_2-NG is the fastest. The monitoring line, situated near the top of the tunnel, records a larger diffusion radius for H_2-NG compared to the central line. This is because, upon reaching the top of the tunnel, the gas collides with the ceiling and disperses laterally, resulting in a wider diffusion radius at the monitoring line.

Fig. 9 presents the impact of leak apertures on the concentration of H_2-NG at different monitoring points. As the leak apertures increase, the mole fraction of the leaking gas also increases, leading to earlier alarm times at monitoring points 8 and 9. When the leak aperture is 2 mm, the H_2-NG mole fraction does not reach the alarm threshold within 100 s of leakage, resulting in a relatively low concentration of gas in the utility tunnel. For leak apertures larger than 8 mm, the H_2-NG quickly approaches the LEL. With an 8 mm leak aperture, monitoring points 8 and 9 reach the LEL at 39 s and 61 s, respectively, and the mole fractions then stabilize at around 6.5% and 5.8%. When the leak aperture is increased to 12 mm, these monitoring points reach the LEL even more rapidly, at 17 s and 24 s, respectively, with subsequent mole fractions stabilizing at 11.8% and 10.2%.

3.3 The influence of HBRs

Fig. 10 illustrates the effect of different HBRs on the concentration of H_2-NG at monitoring point 8 under no mechanical ventilation conditions, with a leak diameter of 2 mm and pipeline pressure of 0.8 MPa. As shown in Fig. 10(a), the mole fraction of the H_2-NG gradually increases with the rise in HBR, and the rate of increase also escalates. This indicates that a higher HBR leads to a greater volume of gas leakage. When the HBR is below 50%, the increase in the mole fraction of H_2-NG leakage is relatively modest. However, as the HBR exceeds 50%, the mole fraction of leaked H_2-NG significantly increases. Fig. 10(b) shows that the rate of growth

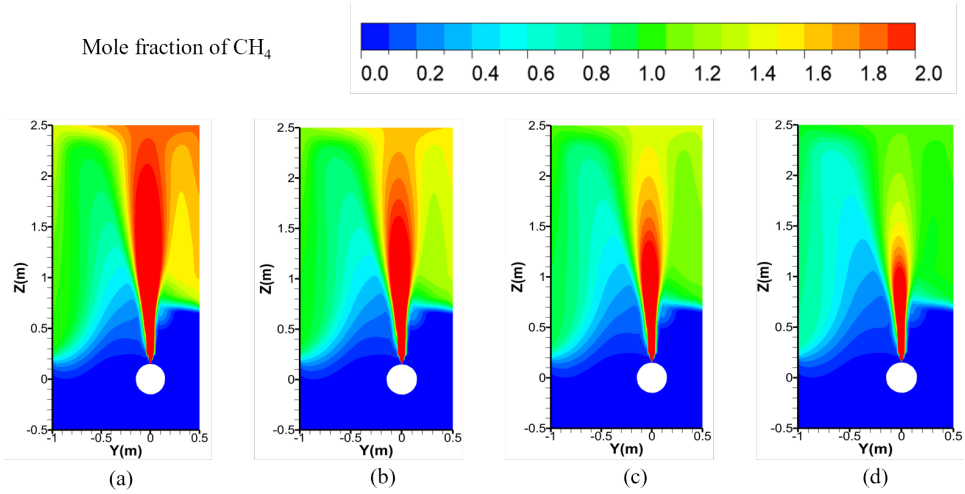

Fig. 11. Natural gas distribution at Y = 0 section with different HBRs at 100 s of leakage: (a) 0%; (b) 10%; (c) 20%; (d) 30%.

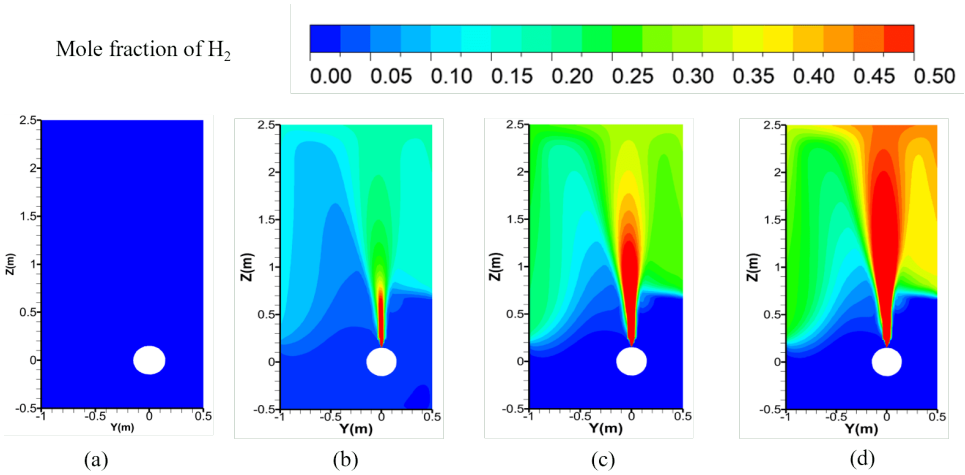

Fig. 12. Hydrogen distribution at Y = 0 section with different HBRs at 100 s of leakage: (a) 0%; (b) 10%; (c) 20%; (d) 30%.

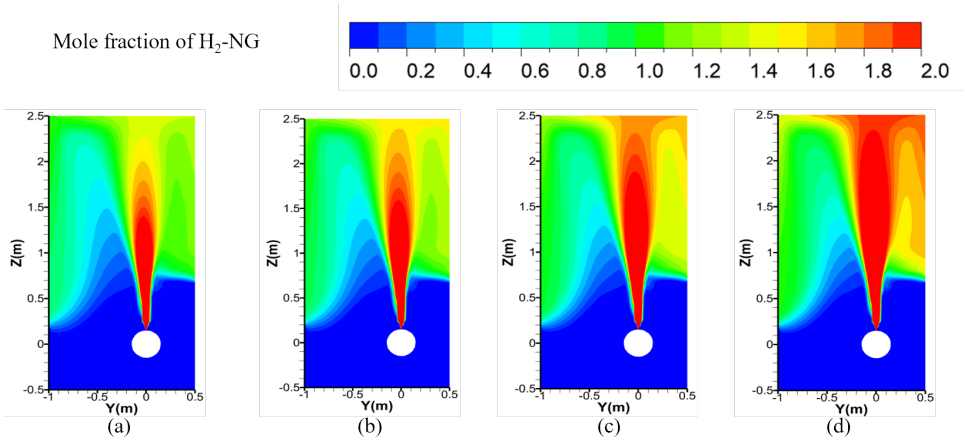

Fig. 13. H_2-NG distribution at Y = 0 section with different HBRs at 100 s of leakage: (a) 0%; (b) 10%; (c) 20%; (d) 30%.

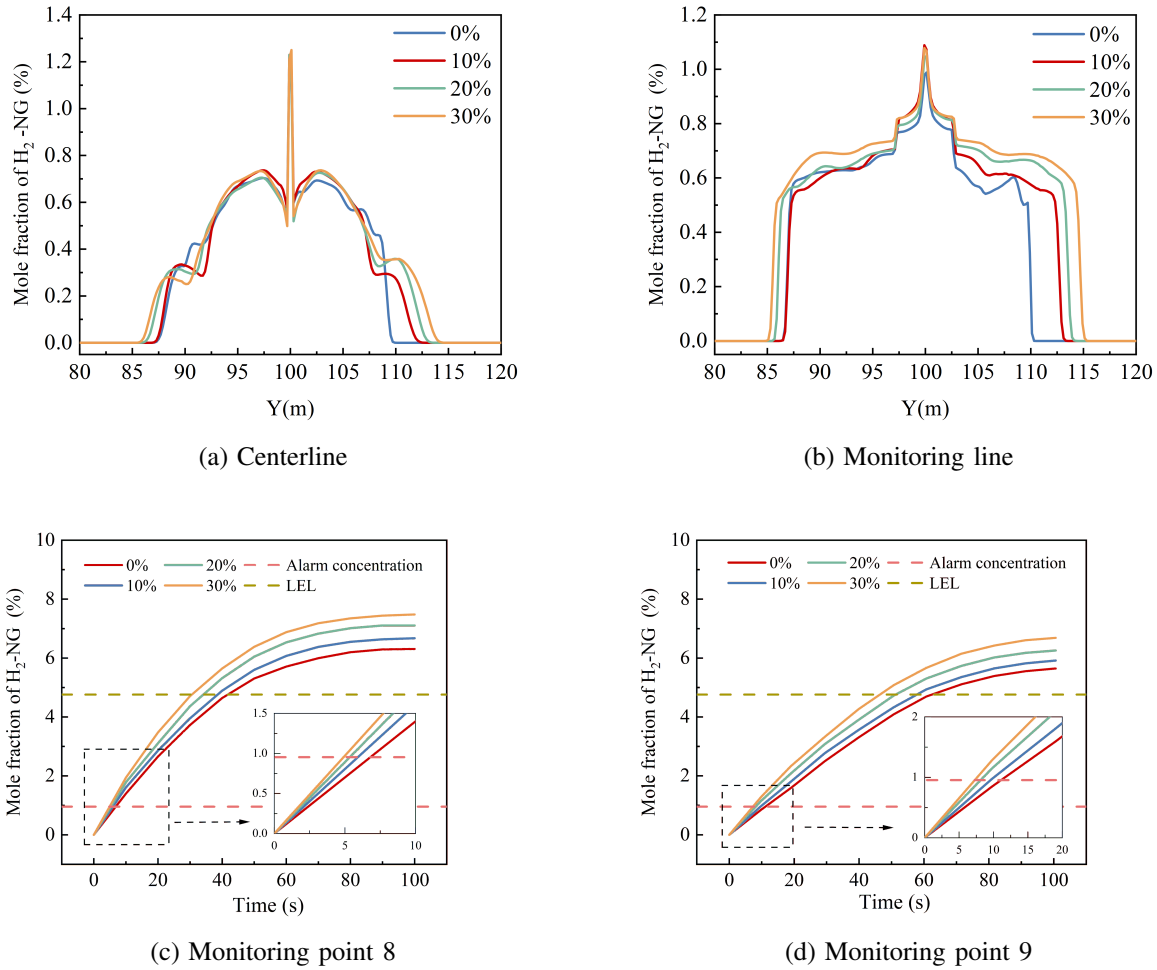

(a) Centerline

(b) Monitoring line

(c) Monitoring point 8

(d) Monitoring point 9

Fig. 14. The effect of HBR on the concentration of H_2-NG.

in the mole fraction of the H_2-NG progressively increases with an increase in HBR. Therefore, at the same leakage duration, both the leakage speed and volume increase with the rise in the HBR. For instance, at t = 100 s compared to a 0% HBR, a 30% HBR results in approximately an 8% increase in H_2-NG mole fraction, whereas a 90% HBR leads to an increase of about 51%. Considering practical applications, subsequent research sets the maximum HBR at 30%. This decision takes into account the balance between the risks associated with higher hydrogen concentrations and the practical feasibility of utility tunnel operations.

To further explore the impact of the HBR on the concentration of the leaking gas, four HBRs of 0%, 10%, 20% and 30% were selected based on the conditions (cases 4, 5, 7 and 8 in Table 2). Figs. 11, 12 and 13 show the distribution of different gases on the Y=0 cross-section at 100 s of leakage under different HBRs. As shown in Fig. 11, which depicts the distribution of natural gas on the Y = 0 cross-section, natural gas jets into the tunnel from the leak hole and accumulates at the top of the tunnel, symmetrically diffusing to both sides and then descending downward. Additionally, with an increasing HBR, the mole fraction of natural gas gradually decreases due to the reduction in the natural gas content in the pipe. As shown in Fig. 12, the diffusion process of hydrogen is similar to that of natural gas, and as the HBR increases, the concentration of hydrogen increases. Fig. 13 shows that the diffusion process of H_2-NG is consistent with that of natural gas and hydrogen. With an increasing HBR, the mole fraction of H_2-NG in the tunnel increases. This is because as the HBR increases, the leaking speed increases, as explained in Fig. 10, leading to a gradual increase in the amount of leakage. The concentration of H_2-NG at the top of the tunnel is greater than that at the bottom.

Fig. 14 illustrates the impact of varying HBRs on the concentration of H_2-NG at different locations. As depicted in Figs. 14(a) and 14(b), an increase in the HBR results in a higher concentration of H_2-NG, yet it has a minimal effect on the diffusion radius. This is primarily because the gas leak speed is much greater than the speed at which the gas diffuses to both sides. Figs. 14(c) and 14(d) demonstrate that as the HBR increases, the alarm times at monitoring points 8 and 9 are advanced. Specifically, for monitoring point 8, which is situated relatively close to the leak source, the alarm time advances from 7.5 seconds to 4.5 seconds as the HBR rises

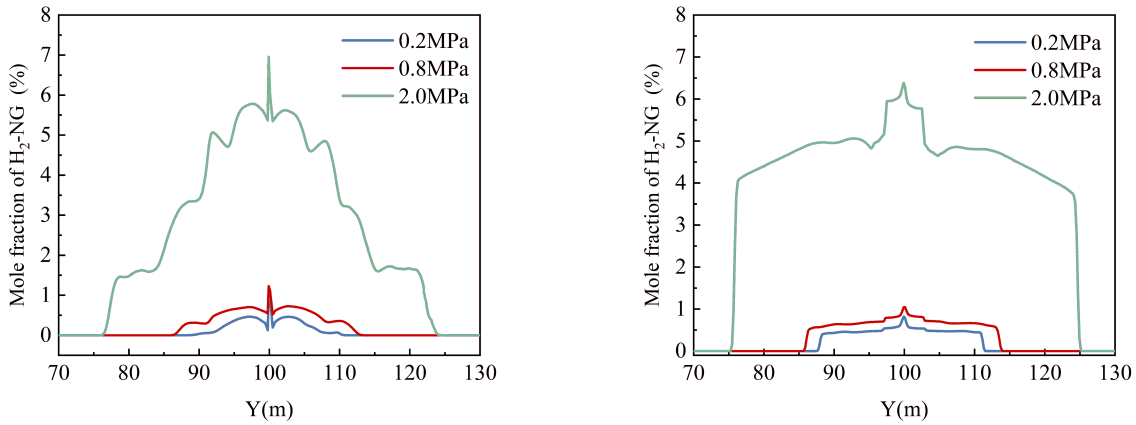

(a) Centerline (b) Monitoring line

Fig. 15. Distribution of H_2-NG at the centerline and monitoring line under different pipeline pressures at t = 100 s.

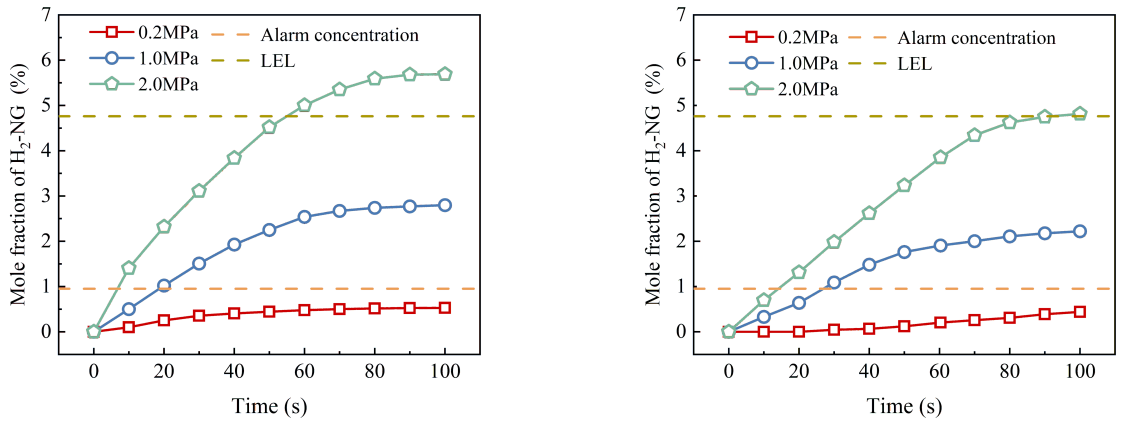

(a) Monitoring point 8 (b) Monitoring point 9

Fig. 16. Effect of pipeline operating pressure on the concentration of H_2-NG.

from 0 to 30%. This advancement in alarm time is attributed to an increase in the volume of H_2-NG as the HBR increases.

3.4 The influence of pipeline operating pressure

Pipeline operating pressure significantly influences the leakage rate of gas, which in turn affects the distribution of gas within the utility tunnels. This section investigates the effect of three operating pressure levels, including 0.2, 1.0 and 2.0 MPa (cases 1, 12 and 13 in Table 2), on the leakage and diffusion behaviors of the leaking gas in the utility tunnel. In these cases, the leak aperture is 2 mm, and the HBR is 20% under no mechanical ventilation conditions.

Fig. 15 illustrates the variation of H_2-NG concentration along the central and the monitoring lines for different operating pressures over time. Observations from Figs. 15(a) and 15(b) reveal that the distribution trends of H_2-NG on both the central and monitoring lines are essentially consistent. Moreover, the higher the operating pressure of the pipeline, the greater the peak mole fraction of H_2-NG and the larger the diffusion radius of the H_2-NG. This increase in the gas mole fraction is because of the greater volume of gas leaked as a result of the elevated pipeline pressure. Specially, with a 2 mm leak aperture, as the pipeline pressure rises from 0.8 MPa to 2.0 MPa, the peak mole fraction of the H_2-NG increases by about 5.5%, and the diffusion radius rises by about 11 m, indicating that pipeline pressure has a significant impact on the leakage and diffusion of H_2-NG.

Fig. 16 illustrates the impact of pipeline operating pressure on the mole fraction of H_2-NG at various monitoring points. With the increase in pipeline operating pressure, the mole fraction of H_2-NG increases correspondingly, leading to earlier alarm times at the monitoring points. For instance, as shown in Fig. 16(b), when the pipeline pressure rises from 1.0 to 2.0 MPa, the alarm time is reduced from 28 to 14 s. When the pipeline operating pressure reaches 2.0 MPa, the concentration of H_2-NG at monitoring points 8 and 9 achieves

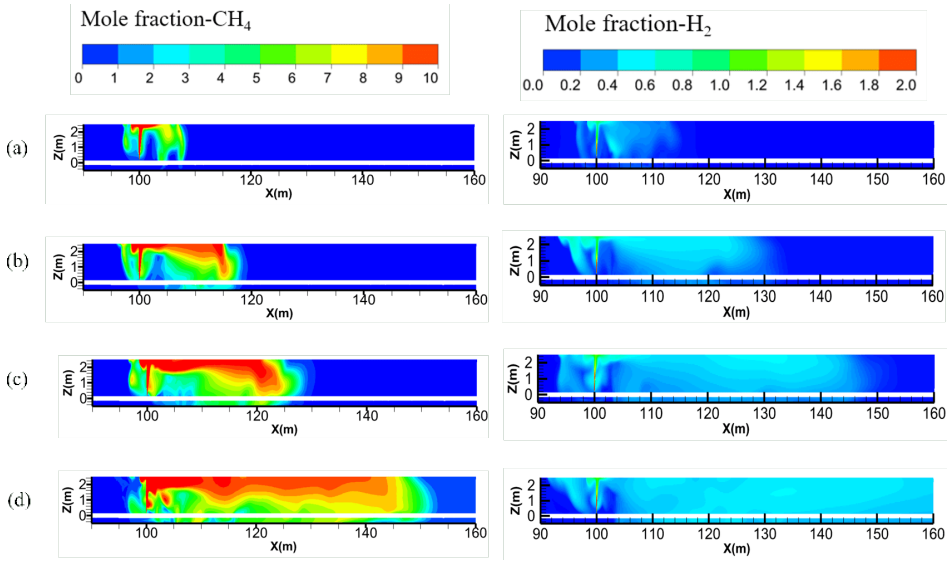

Fig. 17. Effect of ventilation frequencies on the concentration of gases: (a) t = 10 s; (b) t = 30 s; (c) t = 50 s; (d) t = 100 s.

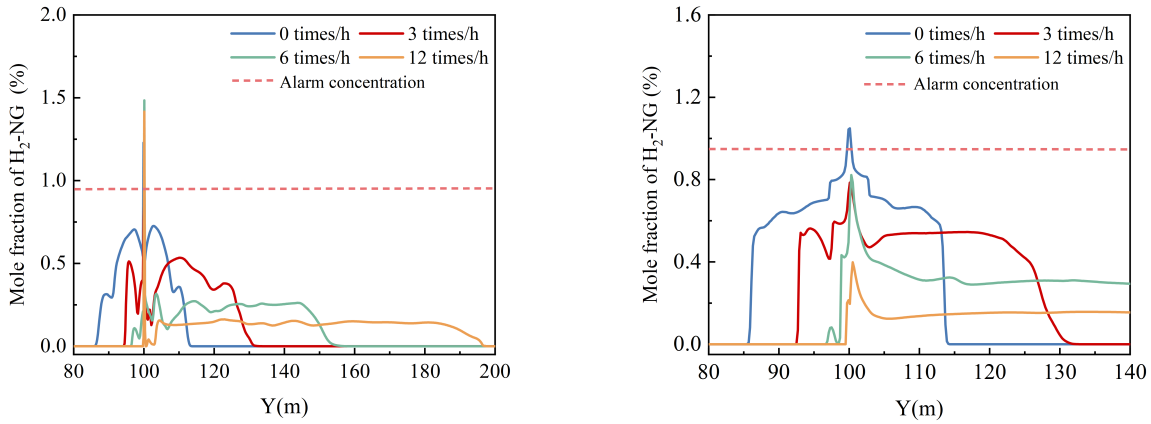

(a) Centerline (b) Monitoring line

Fig. 18. Effect of ventilation frequencies on the H_2-NG distribution.

the LEL at 56 s and 82 s, respectively, whereas at pipeline operating pressures below 1 MPa, monitoring points 8 and 9 do not reach the LEL. Therefore, in the event of a leak in a high-pressure pipeline, gas diffusion within the utility tunnel is faster, necessitating timely measures to reduce the gas concentration.

3.5 The influence of ventilation frequencies

When the mole fraction of leaking gas in utility tunnels reaches the alarm concentration, it is crucial to implement appropriate strategies promptly. Adopting the ventilation strategy can effectively control excessive concentrations of H_2-NG. Different ventilation conditions should be applied for varying leakage apertures, pressures, and HBRs. Therefore, this section explores the impact of varying ventilation frequencies on the distribution of the leaking gas. Fig. 17 shows the time-varying concentration distribution of natural gas and hydrogen in the utility tunnel under a ventilation frequency of 12 times/h, with a leak aperture of 8 mm, pipeline operating pressure of 2 MPa, and an HBR of 20% (case 14 in Table 2). Compared to the scenario without mechanical ventilation (as shown in Fig. 5), the concentration distribution of natural gas and hydrogen on both sides of the leak point clearly shows an asymmetrical trend after mechanical ventilation. Furthermore, mechanical ventilation inhibits the trend of natural gas and hydrogen diffusion upstream in the utility tunnel, reducing the concentration distribution range upstream. Simultaneously, mechanical ventilation increases the airflow rate within the utility tunnel, causing natural gas and hydrogen to diffuse downstream while also reducing their concentrations. This effectively reduces the area of the hazard zone.

Fig. 18 displays the distribution of H_2-NG at various monitoring points for four scenarios: No mechanical ventilation, ventilation 3 times/h, ventilation 6 times/h and ventilation 12

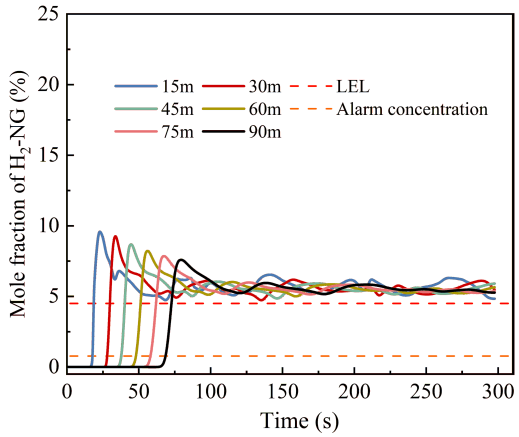

Fig. 19. Concentration of H_2-NG at various points with 12 times per hour ventilation frequencies.

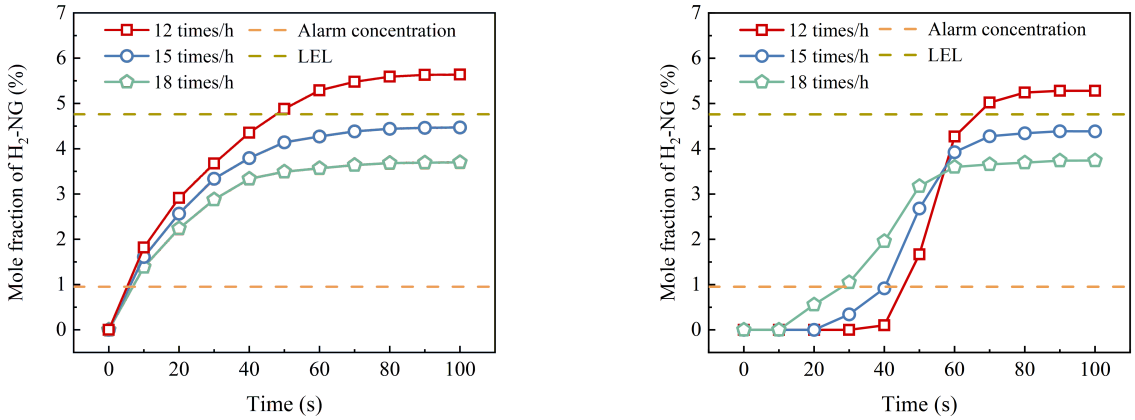

(a) Monitoring point 8

(b) Monitoring point 14

Fig. 20. Effect of ventilation frequencies at different monitoring points on the concentration of H_2-NG.

times/h. These scenarios correspond to cases 7, 9, 10, and 11 in Table 2, with a leakage aperture of 2 mm, pipeline operating pressure of 0.8 MPa, and an HBR of 20%. It is observed that the H_2-NG concentration distribution trends along the central and monitoring lines are consistent. Upon initiating ventilation, the gas diffuses downstream, and the diffusion distance increases with the ventilation frequency. Since the diameter of the leak aperture is only 2 mm, resulting in a relatively small leakage quantity, the mole fraction of the leaking H_2-NG exceeds the alarm threshold only in the area near the leak hole. In other areas, the mole fraction remains below the alarm threshold. Therefore, when the leak aperture is small, adopting a ventilation frequency of 6 to 12 times per hour can effectively reduce the concentration of H_2-NG to a safe range.

Fig. 19 shows the distribution of H_2-NG at various downstream points under a scenario with a leak aperture of 12 mm, pipeline pressure of 0.8 MPa, and an HBR of 20%, where mechanical ventilation at a frequency of 12 times/h is initiated at 10 seconds after the onset of the leak. It is observed that when the leakage aperture is increased to 12 mm, a ventilation frequency of 12 times/h is inadequate to decrease the concentration of the H_2-NG below the LEL. This frequency does not ensure the safe operation of the utility tunnel, indicating the need for a higher frequency of mechanical ventilation to mitigate the risk effectively. Therefore, this study examines the impact of ventilation frequencies of 12, 15 and 18 times/h (cases 14, 15 and 16 in Table 2) for a scenario with a 12 mm aperture, a pipeline pressure of 0.8 MPa, and an HBR of 20%. As shown in Fig. 20(a), near the leak hole, the alarm times under different ventilation conditions are almost the same. However, higher frequency ventilation ($>$ 15 times/h) enables the rapid diffusion of the leaking gas within the utility tunnel, reducing its concentration below the LEL. Fig. 20(b) demonstrates that increasing the ventilation frequency can advance the alarm time at the exit while also reducing the gas concentration to below the LEL. Therefore, when the leakage aperture is large, it is necessary to ensure a minimum ventilation frequency of at least 15 times/h.

4. Conclusions

This paper established a model for the leakage and diffusion of H_2-NG in an underground utility tunnel. Through systematic numerical simulations, it investigated the impact of different factors, such as the size of the leak apertures, pipeline operating pressures, and HBRs, on the distribution of H_2-NG within the tunnel after a leak. Additionally, the study analyzes the influence of ventilation frequency under different aperture sizes on both the alarm time and the time to reach the LEL. The following conclusions were drawn:

1) Under no mechanical ventilation conditions, the H_2-NG disperses symmetrically from the leak point towards both sides of the tunnel, and the concentration and spread radius of the H_2-NG increase with time. The highest concentration of the H_2-NG is near the leak hole, gradually decreasing towards both sides. Increasing pipeline pressure and leak hole size lead to higher H_2-NG concentrations in the tunnel, a larger spread radius, and earlier alarm times. After 100 seconds, when the leak aperture exceeds 8 mm or the pipeline pressure is greater than 2.0 MPa, the concentration of H_2-NG reaches the LEL.
2) Ventilation could effectively reduce gas concentrations within the tunnel and suppress the tendency of gases to spread upstream. For a leak aperture of 2 mm and a pipeline pressure of 0.8 MPa, ventilation frequencies between 6 and 12 times/h can bring gas concentrations within the safe range. However, gas concentrations remain above the LEL for a leak aperture of 12 mm, even with 12 times/h ventilation frequencies. Therefore, it is recommended that the minimum ventilation per hour be increased to 15 times/h or higher in such cases.
3) As the HBR increases, the concentration of the H_2-NG in the upper part of the tunnel gradually rises, and the rate of gas concentration increase also increases, resulting in shorter alarm times. Thus, an increase in the HBR increases the risk of a combustion explosion within the tunnel.

Acknowledgements

This work described herein was supported by the National Key R & D Program of China (2021YFB4001603), the National Natural Science Foundation of China (No. 52006243 and No. 51936001), the Natural Science Foundation of Shandong Province (No. ZR2020QE197), and the Fundamental Research Funds for the Central Universities (No. 22CX06027A).

Conflict of interest

The authors declare no competing interest.

References

Abbas, M. A. H., Kheradmand, S., Sadoughipour, H. Numerical study of the effect of hydrogen leakage position and direction on hydrogen distribution in a closed enclosure. International Journal of Hydrogen Energy, 2020, 45(43): 23872-23881.

Apostolou, D., Xydis, G. A literature review on hydrogen refuelling stations and infrastructure. Current status and future prospects. Renewable and Sustainable Energy Reviews, 2019, 113: 109292.

Choi, J., Hur, N., Kang, S., et al. A CFD simulation of hydrogen dispersion for the hydrogen leakage from a fuel cell vehicle in an underground parking garage. International Journal of Hydrogen Energy, 2013, 38(19): 8084-8091.

El-Ghafour, S. A. A., El-Dein, A. H. E., Aref, A. A. R. Combustion characteristics of natural gas–hydrogen hybrid fuel turbulent diffusion flame. International Journal of Hydrogen Energy, 2010, 35(6): 2556-2565.

Energy Information Authority of the United States Department of Energy (EIA). Natural gas: Coalbed methane reserves and production statistics. Energy Information Authority 2020.

Yu, J., Zhang, H., Jia, W., et al. Numerical Simulation of Leakage and Diffusion in Hydrogen Mixed Natural Gas Transmission Station. Journal of Southwest Petroleum University (Science & Technology Edition), 2022, 44(6): 153-161. (in Chinese)

Kim, E., Park, J., Cho, J. H., et al. Simulation of hydrogen leak and explosion for the safety design of hydrogen fueling station in Korea. International Journal of Hydrogen Energy, 2013, 38(3): 1737-1743.

Kong, M., Feng, S., Xia, Q., et al. Investigation of mixing behavior of hydrogen blended to natural gas in gas network. Sustainability, 2021, 13(8): 4255.

Kong, Y., Li, Y., Wang, S., et al. Experimental study on jet fire characteristics of hydrogen-blended natural gas. International Journal of Hydrogen Energy, 2024, 49: 1250-1260.

Le, T. T., Sharma, P., Bora, B. J., ., et al. Fueling the future: A comprehensive review of hydrogen energy systems and their challenges. International Journal of Hydrogen Energy, 2024, 54: 791-816.

Li, H., Cao, X., Du, H., et al. Numerical simulation of leakage and diffusion distribution of natural gas and hydrogen mixtures in a closed container. International Journal of Hydrogen Energy, 2022, 47(84): 35928-35939.

Li, J., Su, Y., Zhang, H., et al. Research progresses on pipeline transportation of hydrogen-blended natural gas. Natural Gas Industry, 2021, 41(4): 137-152. (in Chinese)

Liu, A., Xu, C., Lu, X., et al. Coupling effect of multiple factors on the diffusion behavior of leaking natural gas in utility tunnels: A numerical study and PIV experimental validation. Gas Science and Engineering, 2023, 118: 205086.

Liu, X. Experimental and Numerical Research on Gas Leak and Diffusion in the Utility Tunnel. Beijing, Beijing Architecture University, 2018. (in Chinese)

Liu, Y., Zheng, J., Xu, P., et al. Numerical simulation on

the diffusion of hydrogen due to high pressured storage tanks failure. Journal of Loss Prevention in the Process Industries, 2009, 22(3): 265-270.

Mei, Y., Shuai, J. Research on natural gas leakage and diffusion characteristics in enclosed building layout. Process Safety and Environmental Protection, 2022, 161: 247-262.

Ogden, J., Jaffe, A. M., Scheitrum, D., et al. Natural gas as a bridge to hydrogen transportation fuel: Insights from the literature. Energy Policy, 2018, 115: 317-329.

Østergaard, P. A., Duic, N., Noorollahi, Y., et al. Latest progress in Sustainable Development using renewable energy technology. Renewable Energy, 2020, 162: 1554-1562.

Østergaard, P. A., Duic, N., Noorollahi, Y., et al. Sustainable development using renewable energy technology. Renewable Energy, 2020a, 146: 2430-2437.

Qian, J., Li, X., Gao, Z., et al. A numerical study of hydrogen leakage and diffusion in a hydrogen refueling station. International Journal of Hydrogen Energy, 2020, 45(28): 14428-14439.

Shao, X., Yang, S., Yuan, Y., et al. Study on the difference of dispersion behavior between hydrogen and methane in utility tunnel. International Journal of Hydrogen Energy, 2022, 47(12): 8130-8144.

Su, Y., Li, J., Yu, B., et al. Numerical investigation on the leakage and diffusion characteristics of hydrogen-blended natural gas in a domestic kitchen. Renewable Energy, 2022, 189: 899-916.

Sun, B., Guo, T. Evidential reasoning and lightweight multi-source heterogeneous data fusion-driven fire danger level dynamic assessment technique. Process Safety and Environmental Protection, 2024, 185: 350-366.

Tian, X., Pei, J. Study progress on the pipeline transportation safety of hydrogen-blended natural gas. Heliyon, 2023, 9.

Wang, F., Zhou, X., Huang, J., et al. Natural gas leakage estimation in underground utility tunnels using Bayesian inference based on flow fields with gas jet disturbance. Process Safety and Environmental Protection, 2022, 165: 532-544.

Wang, L., Chen, J., Ma, T., et al. Numerical study of leakage characteristics of hydrogen-blended natural gas in buried pipelines. International Journal of Hydrogen Energy, 2024, 49: 1166-1179.

Wang, S., Li, Z., Fang, Q., et al. Performance of utility tunnels under gas explosion loads. Tunnelling and Underground Space Technology, 2021, 109: 103762.

Wang, X., Tan, Y., Zhang, T., et al. Diffusion process simulation and ventilation strategy for small-hole natural gas leakage in utility tunnels. Tunnelling and Underground Space Technology, 2020, 97: 103276.

Wu, J., Bai, Y., Fang, W., et al. An integrated quantitative risk assessment method for urban underground utility tunnels. Reliability Engineering & System Safety, 2021, 213: 107792.

Yu, Q., Hou, L., Li, Y., et al. Numerical study on harmful boundary of above-ground section leakage of natural gas pipeline. Journal of Loss Prevention in the Process Industries, 2022, 80: 104901.

Zhao, Y., Wu, J., Zhou, R., et al. Effects of the length and pressure relief conditions on propagation characteristics of natural gas explosion in utility tunnels. Journal of Loss Prevention in the Process Industries, 2022, 75: 104679.

Zhou, K., Li, F., Cai, H., et al. Estimation of the natural gas leakage source with different monitoring sensor networks in an underground utility Tunnel: From the perspectives of energy security. Energy and Buildings, 2022, 254: 111645.